

## Measurement of eight scalar and dipolar couplings for methine–methylene pairs in proteins and nucleic acids

Emeric Miclet<sup>a,b</sup>, Jérôme Boisbouvier<sup>a,c</sup> & Ad Bax<sup>a</sup>

<sup>a</sup>Laboratory of Chemical Physics, National Institute of Diabetes and Digestive and Kidney Diseases, National Institutes of Health, Bethesda, Maryland, 20892-0520; <sup>b</sup>Present address: Laboratoire Structure et Fonction de Molécules Bioactives, UMR 7613 – Université Pierre et Marie Curie, 4, Place Jussieu, 75252, Paris Cedex 5, France; <sup>c</sup>Present address: Laboratoire de RMN, Institut de Biologie Structurale – Jean-Pierre Ebel, UMR 5075 CNRS-CEA-UJF, 41 rue Jules Horowitz, 38027, Grenoble, Cedex 1, France

Received 08 October 2004; Accepted 20 December 2004

**Key words:** alignment, dipolar coupling, E.COSY, liquid crystal, methylene, scalar coupling, side chain conformation

### Abstract

A new 3D, spin-state-selective coherence transfer NMR experiment is described that yields accurate measurements for eight scalar or dipolar couplings within a spin system composed of a methylene adjacent to a methine group. Implementations of the experiment have been optimized for proteins and for nucleic acids. The experiments are demonstrated for C<sup>β</sup>–C<sup>α</sup> moieties of the third IgG-binding domain from Streptococcal Protein G (GB3) and for C<sup>5'</sup>–C<sup>4'</sup> groups in a 24-nt RNA oligomer. Chemical shifts of C<sup>α</sup>, C<sup>β</sup> and H<sup>β</sup> (respectively C<sup>4'</sup>, C<sup>5'</sup> and H<sup>5'</sup>) are dispersed in the three orthogonal dimensions, and the absence of heteronuclear decoupling leads to distinct and well-resolved E.COSY multiplet patterns. In an isotropic sample, the E.COSY displacements correspond to  $^1J_{C^{\alpha}H^{\alpha}}$ ,  $^2J_{C^{\alpha}H^{\beta}2} + ^2J_{C^{\alpha}H^{\beta}3}$ ,  $^2J_{C^{\beta}H^{\alpha}}$ ,  $^1J_{C^{\beta}H^{\beta}2} + ^1J_{C^{\beta}H^{\beta}3}$ ,  $^1J_{C^{\beta}H^{\beta}2} - ^2J_{H^{\beta}2H^{\beta}3}$ ,  $^1J_{C^{\beta}H^{\beta}3} - ^2J_{H^{\beta}2H^{\beta}3}$ ,  $^3J_{H^{\alpha}H^{\beta}2}$  and  $^3J_{H^{\alpha}H^{\beta}3}$  for proteins, and  $^1J_{C^{4'}H^{4'}}$ ,  $^2J_{C^{4'}H^{5'}} + ^2J_{C^{4'}H^{5''}}$ ,  $^2J_{C^{5'}H^{4'}}$ ,  $^1J_{C^{5'}H^{5'}} + ^1J_{C^{5'}H^{5''}}$ ,  $^1J_{C^{5'}H^{5'}} - ^2J_{H^{5'}H^{5''}}$ ,  $^1J_{C^{5'}H^{5''}} - ^2J_{H^{5'}H^{5''}}$ ,  $^3J_{H^{4'}H^{5'}}$  and  $^3J_{H^{4'}H^{5''}}$  in nucleic acids. The experiment, based on relaxation-optimized spectroscopy, yields best results when applied to residues where the methine–methylene group corresponds to a reasonably isolated spin system, as applies for C, F, Y, W, D, N and H residues in proteins, or the C<sup>5'</sup>–C<sup>4'</sup> groups in nucleic acids. Splittings can be measured under either isotropic or weakly aligned conditions, yielding valuable structural information both through the <sup>3</sup>J couplings and the one-, two- and three-bond dipolar interactions. Dipolar couplings for 10 out of 13 sidechains in GB3 are found to be in excellent agreement with its X-ray structure, whereas one residue adopts a different backbone geometry, and two residues are subject to extensive  $\chi_1$  rotamer averaging. The abundance of dipolar couplings can also yield stereospecific assignments of the non-equivalent methylene protons. For the RNA oligomer, dipolar data yielded stereospecific assignments for six out of the eight C<sup>5'</sup>H<sub>2</sub> groups in the loop region of the oligomer, in all cases confirmed by  $^1J_{C^{5'}H^{5'}} > ^1J_{C^{5'}H^{5''}}$ , and H<sup>5'</sup> resonating downfield of H<sup>5''</sup>.

### Introduction

Three-, two- and one-bond J couplings have long been used as a valuable source of information in NMR structural studies of polypeptides and nucleic acids (Bystrov, 1976; Hansen, 1981; Bax

et al., 1994; Biamonti et al., 1994; Ippel et al., 1996; Marino et al., 1999; Schmidt et al., 1999). More recently, methods that impose weak alignment relative to the magnetic field have become available, which result in non-zero values for the corresponding dipolar interactions (Tolman et al., 1995;

Tjandra and Bax, 1997; Clore et al., 1998; Hansen et al., 1998; Ruckert and Otting, 2000; Sass et al., 2000; Tycko et al., 2000). Their measurement makes available a wealth of additional, independent information that is readily incorporated in structure calculations (Tjandra et al., 1997; Meiler et al., 2000; Mueller et al., 2000; Sass et al., 2001). Since all dipolar interactions relate to the orientation of the corresponding internuclear vector relative to a global alignment frame, they nicely complement NOE and J coupling interactions, which measure pairwise distances and local dihedral properties, respectively. Mostly, the residual dipolar couplings (RDCs) in weakly aligned systems are measured by the same methods that are commonly used for quantifying the corresponding J couplings. Besides simple measurement of splittings in 1D or 2D NMR spectra, the most widely used methods for measuring these interactions are either of the E.COSY-type (Griesinger et al., 1986; Biamonti et al., 1994), or involve so-called quantitative J correlation, where the value of the coupling follows from the intensity ratio for a correlation between the nuclei in question and a reference intensity (Bax et al., 1994; Meier et al., 2003). The present study relies on E.COSY-type measurement of interactions.

Frequently, separate experiments are conducted to measure different types of J couplings (Prestegard et al., 2004). For example, experiments have been proposed that optimize measurement of the one-bond  $^{15}\text{N}-^1\text{H}^{\text{N}}$  couplings in backbone amides (Tjandra et al., 1996; Tolman and Prestegard, 1996), the  $^1\text{H}^{\text{N}}-^1\text{H}^{\alpha}$  coupling in peptides (Montelione and Wagner, 1989; Kuboniwa et al., 1994), or the  $^{13}\text{C}-^1\text{H}_3$  couplings in methyl groups (Kontaxis and Bax, 2001), etc. When measuring couplings with E.COSY type techniques, generally requiring at least three coupled nuclei (A, B and C), only correlations between directly connected transitions of nuclei A and B are present in the corresponding cross-multiplet. Components are displaced in one dimension by the A-C interaction and in the other dimension by the B-C coupling. For the application to measurement of J couplings, historically most interest has been in the measurement of three-bond interactions, e.g., B-C, where A-C is a relatively large one- or two-bond interaction that separates the otherwise overlapping B-C multiplet components, with  $J_{\text{AC}}$  itself often being of little interest. In contrast, when

measuring RDCs, all interactions carry meaningful information. Among the many examples of such measurements we mention simultaneous E.COSY measurement of the  $^1\text{H}^{\text{N}}-^{13}\text{C}'$  and  $^{15}\text{N}-^{13}\text{C}'$  couplings (Wang et al., 1998; Yang et al., 1999), and of the  $^{13}\text{C}^{\alpha}-^1\text{H}^{\text{N}}$  and  $^{13}\text{C}^{\alpha}-^{13}\text{C}'$  couplings (Yang et al., 1999; Permi et al., 2000). In favorable cases, up to three couplings can be measured from such an E.COSY multiplet. For example, when recording a 2D  $^1\text{H}-^{15}\text{N}$  correlation with  $^{13}\text{C}^{\alpha}$  but without  $^{13}\text{C}'$  decoupling, the  $^{15}\text{N}$  dimension shows splittings by both the one-bond  $^{15}\text{N}-^1\text{H}$  and the one-bond  $^{15}\text{N}-^{13}\text{C}'$  couplings, whereas the multiplet components are displaced by the two-bond  $^{13}\text{C}'-^1\text{H}^{\text{N}}$  coupling in the  $^1\text{H}^{\text{N}}$  dimension (Wang et al., 1998).

When correlating three spins of a four-spin system along the three axes of a 3D spectrum, the E.COSY properties can be used to measure up to six couplings for a given correlation. For example, five scalar and dipolar couplings were measured at good accuracy for fragments of two adjacent  $^{13}\text{C}-^1\text{H}$  groups, as applies for the  $\text{C}^1\text{H}$  and  $\text{C}^2\text{H}$  groups in  $^{13}\text{C}$ -enriched RNA. These couplings included  $\text{C}^1-\text{H}^1$ ,  $\text{C}^2-\text{H}^2$ ,  $\text{C}^1-\text{H}^2$ ,  $\text{C}^2-\text{H}^1$ , and  $\text{H}^2-\text{H}^1$ , but not the  $\text{C}^1-\text{C}^2$  splitting, which was removed for enhancing sensitivity and minimizing spectral overlap (O'Neil-Cabello et al., 2004).

Here, we describe and demonstrate analogous methods for simultaneous measurement of eight couplings from the 3D correlation between  $\text{C}^{\beta}-\text{H}^{\beta}_2$  and  $\text{C}^{\alpha}-\text{H}^{\alpha}$  for methylene groups adjacent to a methine site (five-spin system). The resulting spectrum yields values for  $^1J_{\text{C}^{\alpha}\text{H}^{\alpha}}$ ,  $^2J_{\text{C}^{\alpha}\text{H}^{\beta}_2} + ^2J_{\text{C}^{\alpha}\text{H}^{\beta}_3}$ ,  $^2J_{\text{C}^{\beta}\text{H}^{\alpha}}$ ,  $^1J_{\text{C}^{\beta}\text{H}^{\beta}_2}$ ,  $^1J_{\text{C}^{\beta}\text{H}^{\beta}_3}$ ,  $^2J_{\text{H}^{\beta}_2\text{H}^{\beta}_3}$ ,  $^3J_{\text{H}^{\alpha}\text{H}^{\beta}_2}$ , and  $^3J_{\text{H}^{\alpha}\text{H}^{\beta}_3}$  in  $^{13}\text{C}$ -enriched proteins, and analogous couplings in nucleic acids when considering the  $\text{C}^4-\text{C}^5$  methine-methylene pair. Although the experiment only measures the sum,  $^2J_{\text{C}^{\alpha}\text{H}^{\beta}_2} + ^2J_{\text{C}^{\alpha}\text{H}^{\beta}_3}$ , and not the individual couplings for the  $\text{C}^{\alpha}-\text{H}^{\beta}$  interaction, when considering the sum of the dipolar couplings this is readily incorporated as a dipolar restraint in structure calculation (Ottiger et al., 1998), with a restraining power comparable to that of an individual  $\text{C}^{\alpha}-\text{H}^{\beta}$  interaction. The measurement of such a large number of couplings for a small sidechain or phospho-diester backbone fragment, in combination with experimental restraints available from other parameters for the remainder of the backbone, can yield more parameters than degrees of freedom, when assum-

ing a single static structure with idealized covalent geometry. Therefore, the simultaneous measurement of such a large number of couplings also holds potential for identifying motional properties, such as sidechain rotamer averaging or backbone rearrangements (Mittermaier and Kay, 2001; Tolman, 2001; Tolman et al., 2001; Chou et al., 2003), complementing the sidechain rotamer information available from the isotropic  $^3J_{\text{HH}}$  couplings.

## Methods

Four samples were employed in this study, which comprise the isotropic and anisotropic phases of the 1.5 mM uniformly ( $>95\%$ )  $^{13}\text{C}$ ,  $^{15}\text{N}$ -labelled third IgG-binding domain from Streptococcal Protein G, hereafter referred to as GB3, and the 1.9 mM uniformly  $^{13}\text{C}$ -enriched RNA stem-loop oligomer, mimicking nucleotides 737–760 of *E. coli* 23S ribosomal RNA and modified to contain  $\psi_{746}$ , hereafter referred to as RNA oligomer. The isotropic GB3 sample contained 99%  $\text{D}_2\text{O}$ , 50 mM sodium phosphate, pH 5.6. The anisotropic GB3 sample contained 7%  $\text{D}_2\text{O}$ , 40 mM sodium phosphate, pH 6.5, 0.08%  $\text{NaN}_3$ , and 10 mg/ml Pf1 phage, strain LP11-92 (ASLA, Ltd., Latvia) to induce alignment of the protein (Hansen et al., 1998). Both RNA oligomer samples were in 99%  $\text{D}_2\text{O}$ , 10 mM NaCl, 10 mM phosphate, pH 6.8, 0.02 mM EDTA, and 20 mg/ml liquid crystalline Pf1 for the anisotropic sample.

All NMR experiments were carried out at 25 °C on Bruker spectrometers equipped with a room-temperature, triple resonance, three-axis pulsed-field-gradient probehead, optimized for  $^1\text{H}$  detection. The spectrum of the isotropic GB3 sample was recorded at 750 MHz and results from a  $70^* \times 122^* \times 1024^*$  data matrix, with acquisition times of 24 ms ( $t_1$ ), 37 ms ( $t_2$ ) and 100 ms ( $t_3$ ), respectively. A relaxation delay of 1 s was used. For each hypercomplex  $t_1/t_2$  increment the number of scans was 16, leading to a total measuring time of 46 h. The spectrum of the anisotropic GB3 sample was recorded at 800 MHz and results from a  $50^* \times 145^* \times 1024^*$  data matrix with acquisition times of 20 ms ( $t_1$ ), 40 ms ( $t_2$ ) and 100 ms ( $t_3$ ), respectively. A relaxation delay of 0.7 s was used. For each hypercomplex  $t_1/t_2$  increment the total number of scans was 32, leading to a total measuring time of 58 h. Two interleaved spectra

were recorded for each RNA oligomer sample, at a  $^1\text{H}$  frequency of 750 MHz. For the isotropic sample, two matrices of  $36^* \times 56^* \times 512^*$  data points were collected with corresponding acquisition times of 23 ms ( $t_1$ ), 36 ms ( $t_2$ ) and 85 ms ( $t_3$ ). A relaxation delay of 0.9 s was used, with 48 scans for each hypercomplex  $t_1/t_2$  increment. The total measuring time was 57 h. For the anisotropic sample, two matrices of  $36^* \times 18^* \times 512^*$  data points were collected at 800 MHz, with corresponding acquisition times of 23 ms ( $t_1$ ), 13 ms ( $t_2$ ) and 85 ms ( $t_3$ ). A relaxation delay of 1 s was used with 64 scans for each hypercomplex  $t_1/t_2$  increment. The total measuring time was 24 h. All data sets were processed with nmrPipe (Delaglio et al., 1995). Shifted sine-bell and shifted squared sine-bell window functions were applied in the indirectly and directly detected dimensions, respectively. Data were extensively zero-filled prior to Fourier transformation to yield high digital resolution.

## Results and discussion

The experiments described below for simultaneous measurement of the eight  $^1\text{J}$ ,  $^2\text{J}$  and  $^3\text{J}$  splittings involving an adjacent methylene–methine pair are of the “out-and-back” type (Ikura et al., 1990). Optimal implementations differ slightly for proteins and nucleic acids, although conceptually they are very similar. In both cases, best results are obtained with magnetization starting out on the methylene site, resulting in an HBCBCA experiment for proteins and an  $\text{H}^5\text{C}^5\text{C}^4$  experiment for nucleic acids. Uni-directional experiments, where magnetization starts out on the methine site, are also possible but yield lower sensitivity for the molecules investigated. We therefore restrict our discussion to the out-and-back experiments, starting from the methylene site. Our analysis below is restricted to the case of weak coupling between the methylene protons ( $\nu_{\text{H1}} - \nu_{\text{H2}} \gg ^2J_{\text{H1H2}}$ ), although in practice we find selectivity to remain good even in the case of moderately strong coupling ( $\nu_{\text{H1}} - \nu_{\text{H2}} \approx 5 \times ^2J_{\text{H1H2}}$ ).

### *H<sup>α</sup>-coupled HBCBCA experiment*

Figure 1a shows the pulse sequence of a 3D experiment that allows the simultaneous measurement of eight couplings in proteins:  $^1J_{\text{C}\alpha\text{H}\alpha}$ ,

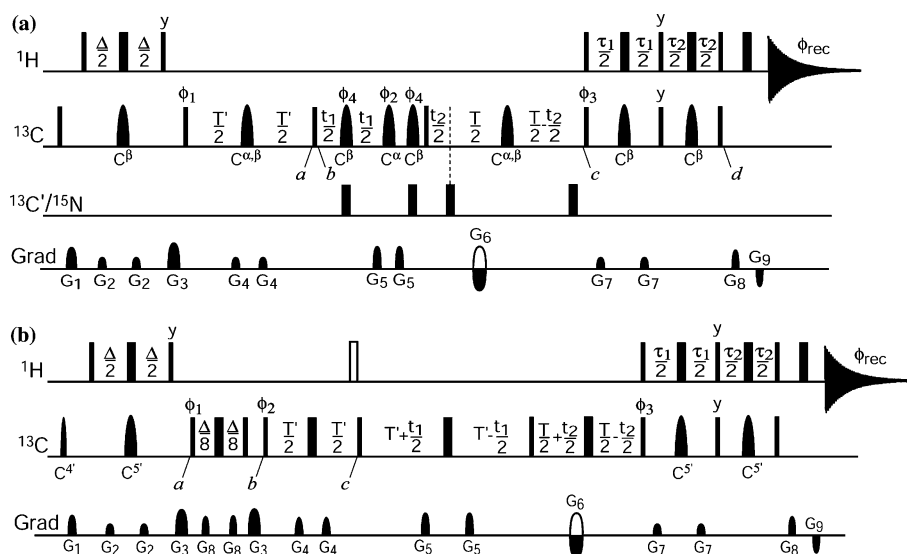


**Figure 1.** Pulse schemes of the 3D spin-state-selective experiments. Narrow and wide bars indicate non-selective  $90^\circ$  and  $180^\circ$  pulses, respectively. Unless specified, pulse phases are  $x$ . Experiments are recorded in the regular Rance-Kay manner (Kay et al., 1992): for each  $t_1$  increment two FIDs are acquired, one with  $G_6$  and  $\phi_3$  inverted, and stored separately. Field gradients are sine-bell shaped with durations  $G_{1,\dots,9}$  of 1, 0.6, 1, 2, 0.2, 2, 0.3, 0.35, 0.153 ms, and  $z$  axis amplitudes of 10, 18, 12, 7, 25,  $-30$ , 17, 30,  $-30$  G/cm. The absence of  $^{13}\text{C}$  decoupling during detection allows the use of long acquisition times (ca. 120 ms). (a) Pulse scheme of the  $\text{H}^\alpha$ -coupled spin-state selective HBCBCA experiment. The shaped  $^{13}\text{C}^\alpha$  (carrier at 54 ppm),  $^{13}\text{C}^\beta$  (carrier at 38 ppm), and  $^{13}\text{C}^{\alpha,\beta}$  (carrier at 45 ppm) pulses have REBURP (Geen and Freeman, 1991) profiles (with respective durations of 2.5, 1.5, and 0.4 ms, for 8, 14, and 48 ppm bandwidth inversions at 750 MHz). Two different  $^{13}\text{C}'$  shaped pulses are employed, a  $370\ \mu\text{s}$  IBURP profile applied at 175 ppm (45 ppm bandwidth inversion at 750 MHz), and a  $800\ \mu\text{s}$  hyperbolic secant pulse (carrier at 150 ppm; 110 ppm bandwidth inversion at 750 MHz) when both  $^{13}\text{C}'$  and  $^{13}\text{C}^{\text{arom}}$  spins need to be decoupled during the  $^{13}\text{C}^\beta$  evolution. Delay durations:  $\Delta = 1/(2J_{\text{C}^\alpha\text{H}^\beta}) \approx 3.6$  ms;  $T' = 1/(2J_{\text{C}^\alpha\text{C}^\beta}) \approx 14$  ms;  $T = 1/(2J_{\text{C}^\alpha\text{C}^\beta})$  or  $3/(2J_{\text{C}^\alpha\text{C}^\beta})$ ;  $\tau_1 = 0.34/(J_{\text{C}^\beta\text{H}^\beta}) \approx 2.5$  ms;  $\tau_2 = 0.23/(J_{\text{C}^\beta\text{H}^\beta}) \approx 1.65$  ms. Phases:  $\phi_1 = y, -y$ ;  $\phi_2 = x, x, y, y$ ;  $\phi_3 = x$ ;  $\phi_4 = x, y, -x, -y$ ; and  $\phi_{\text{rec}} = x, -x, -x, x$ . (b) Pulse scheme of the  $\text{H}^\alpha$ -coupled spin-state selective  $\text{H}^\alpha\text{C}^\alpha\text{C}^\beta$  experiment. The initial  $^{13}\text{C}^\alpha$   $90^\circ$  shaped pulse has a Gaussian  $G_4$  profile (Emsley and Bodenhausen, 1990) (carrier at 83.5 ppm, 5 ms for a 7 ppm bandwidth excitation at 750 MHz). The  $^{13}\text{C}^\beta$  (carrier at 66 ppm) pulses have REBURP profiles (1.8 ms at 750 MHz for a 11 ppm inversion bandwidth). Phases:  $\phi_1 = 135^\circ, -45^\circ$ ;  $\phi_2 = y, y, -y, -y$ ;  $\phi_3 = x$ ;  $\phi_{\text{rec}} = x, -x, -x, x$ . Delay durations:  $\Delta = 1/(2J_{\text{C}^\beta\text{H}^\beta}) \approx 3.4$  ms;  $T' = 1/(2J_{\text{C}^\alpha\text{C}^\beta}) \approx 12.5$  ms;  $T = 1/(2J_{\text{C}^\alpha\text{C}^\beta})$  or  $3/(2J_{\text{C}^\alpha\text{C}^\beta})$ . A  $220\ \mu\text{s}$  duration is added to  $\text{CH}_2\text{-S}^3\text{CT}$  delays  $\tau_1$  and  $\tau_2$  ( $\tau_1 = 0.34/J_{\text{C}^\beta\text{H}^\beta}$  and  $\tau_2 = 0.23/J_{\text{C}^\beta\text{H}^\beta}$ ) to take into account the incomplete  $J_{\text{C}^\beta\text{H}^\beta}$  evolution during the  $^{13}\text{C}^\beta$  REBURP pulses: The open  $^1\text{H}$   $180^\circ$  pulse is only applied when selecting the upfield  $^{13}\text{C}^\beta$  triplet component. Corresponding Bruker pulse programs and processing scripts are available at <http://spin.niddk.nih.gov/bax/>.

${}^2J_{\text{C}^\alpha\text{H}^\beta 2} + {}^2J_{\text{C}^\alpha\text{H}^\beta 3}$ ,  ${}^2J_{\text{C}^\beta\text{H}^\alpha}$ ,  ${}^1J_{\text{C}^\beta\text{H}^\beta 2}$ ,  ${}^1J_{\text{C}^\beta\text{H}^\beta 3}$ ,  ${}^2J_{\text{H}^\beta 2\text{H}^\beta 3}$ ,  ${}^3J_{\text{H}^\alpha\text{H}^\beta 2}$  and  ${}^3J_{\text{H}^\alpha\text{H}^\beta 3}$ . The pulse scheme is an extension of the recently proposed 2D  $\text{CH}_2\text{-TROSY}$  experiment (Miclet et al., 2004), using an additional frequency dimension ( $^{13}\text{C}^\alpha$ ) to reveal new couplings involving  $^{13}\text{C}^\alpha$  and  $^1\text{H}^\alpha$ . Conceptually, the experiment is also closely related to an experiment described by Carlomagno et al., (2000). The experiment correlates the chemical shifts of  $^{13}\text{C}^\alpha$  ( $t_1$ ),  $^{13}\text{C}^\beta$  ( $t_2$ ) and  $^1\text{H}^\beta$  ( $t_3$ ), in the absence of heteronuclear decoupling. Values for the couplings are then extracted from 3D E.COSY-type cross peak multiplets (Griesinger et al., 1986), centered at  $\{^{13}\text{C}^\alpha, ^{13}\text{C}^\beta, ^1\text{H}^\beta\}$  and  $\{^{13}\text{C}^\alpha, ^{13}\text{C}^\beta, ^1\text{H}^\beta\}$  chemical shifts, respectively.

In Figure 1a, magnetization is initially transferred from  $\text{H}^\beta$  to  $\text{C}^\alpha$  by means of two sequential

INEPT steps. Depending on the amino acid type, different product operators (Sørensen et al., 1983) describe the spin coherence at time  $a$ :  $4C_z^\alpha H_z^\beta C_y^\beta$  for C, F, Y, W, D, N, H (group I);  $8C_z^\alpha C_z^\gamma H_z^\beta C_x^\beta$  for T, L, M, P, E, Q, K, R (group II); and  $16C_z^\alpha C_z^\gamma C_z^\gamma H_z^\beta C_y^\beta$  for I and V (group III). For group I, the subsequent  $90_x^\circ$   $^{13}\text{C}$  pulse (time  $a$ ) transforms the operator  $4C_z^\alpha H_z^\beta C_y^\beta$  into the single quantum coherence  $-4C_z^\beta H_z^\beta C_x^\alpha$  whereas multiple quantum coherences are generated for the other two groups. Coherences associated with groups II and III are partially destroyed by the phase-cycled selective  $^{13}\text{C}^\alpha$   $180^\circ$  pulse, flanked by the two gradients  $G_5$ . The residual, unsuppressed components give rise to correlations that are about an order of magnitude weaker than those of group I residues. These group II and III correlations fall

in a spectral region quite different from group I correlations, which mostly have a more downfield  $H^\beta$  chemical shift. Therefore, these residual signals usually are easily recognized and do not interfere with detection and analysis of couplings for residues of group I. As the  $^{13}\text{C}^\beta$  spectral region extensively overlaps with that of other aliphatic sidechain carbons, numerous other terms are also generated at time point  $b$ . However, none of these carries  $C_x^\alpha$  or  $C_y^\alpha$  term, and they therefore are eliminated by the phase-cycled selective  $^{13}\text{C}^\alpha$   $180^\circ$  pulse. This is particularly important for the intense  $\text{C}^\epsilon\text{H}_2$  signals of Lys residues, which resonate in the same spectral region as the  $\text{C}^\beta\text{H}_2$  of group I. Finally, by eliminating the  $^{13}\text{C}$  Boltzmann magnetization prior to the start of the experiment, signals from Gly and Ala residues can be removed from the spectrum.

Thus, only the  $4C_z^\beta H_z^\beta C_y^\alpha$  term of group I residues is retained after  $t_1$  evolution in a  $^{13}\text{C}^\beta$ -decoupled,  $^1\text{H}$ -coupled mode. Taking into account the three couplings  $^1J_{\text{C}\alpha\text{H}\alpha}$ ,  $^2J_{\text{C}\alpha\text{H}\beta 2}$  and  $^2J_{\text{C}\alpha\text{H}\beta 3}$  that are active during this period, eight single transitions  $C_{pqr}^\alpha$  can be distinguished during  $t_1$ , where  $p$ ,  $q$  and  $r$  denote “+” (corresponding to eigenstate  $|\alpha\rangle$ ) or “-” (corresponding to eigenstate  $|\beta\rangle$ ), and refer to the spin states of  $^1\text{H}^{\beta 2}$ ,  $^1\text{H}^{\beta 3}$  and  $^1\text{H}^\alpha$ , respectively (Figure 2a). Evolution resulting from coupling between  $\text{C}^\alpha$  and  $\text{C}'$ ,  $\text{C}^\beta$ , and  $^{15}\text{N}$  is refocused at the mid-point of  $t_1$ , in order to enhance sensitivity. At the end of the  $t_1$  evolution period,  $-4C_z^\beta H_z^\beta C_y^\alpha$  is converted back into transverse  $\text{C}^\beta$  magnetization:  $4C_z^\alpha H_z^\beta C_y^\beta$ . At time point  $c$ , this operator has evolved in a constant-time mode and has been refocused with respect to  $^1J_{\text{C}\alpha\text{C}\beta}$ , yielding  $2H_z^\beta C_x^\beta$ . In the  $\text{C}^\beta$  dimension, eight transitions can be distinguished (denoted  $C_{pqr}^\beta$  where  $p$ ,  $q$ , and  $r$  again refer to the spin states of  $^1\text{H}^{\beta 2}$ ,  $^1\text{H}^{\beta 3}$  and  $^1\text{H}^\alpha$ ). However, it can be shown that the four multiplet components corresponding to transitions  $C_{+-+}^\beta$ ,  $C_{+--}^\beta$ ,  $C_{-+-}^\beta$  and  $C_{--+}^\beta$  cancel one another. The absence of  $^1\text{H}$  pulses between the  $^{13}\text{C}$   $t_1$  and  $t_2$  evolution periods preserves the  $^1\text{H}^{\beta 2}$ ,  $^1\text{H}^{\beta 3}$  and  $^1\text{H}^\alpha$  spin states, and results in specific correlations between four pairs of single transitions  $C_{pqr}^\alpha$  and  $C_{pqr}^\beta$  (as mentioned above, only transitions for which  $p=q$  are observable).

Analogous to the  $^{13}\text{C}$  case, and taking into account the three couplings  $^1J_{\text{C}\beta\text{H}\beta 2}$ ,  $^2J_{\text{H}\beta 2\text{H}\beta 3}$  and  $^3J_{\text{H}\alpha\text{H}\beta 2}$ , eight single transitions  $H_{pqr}^{\beta 2}$  can be

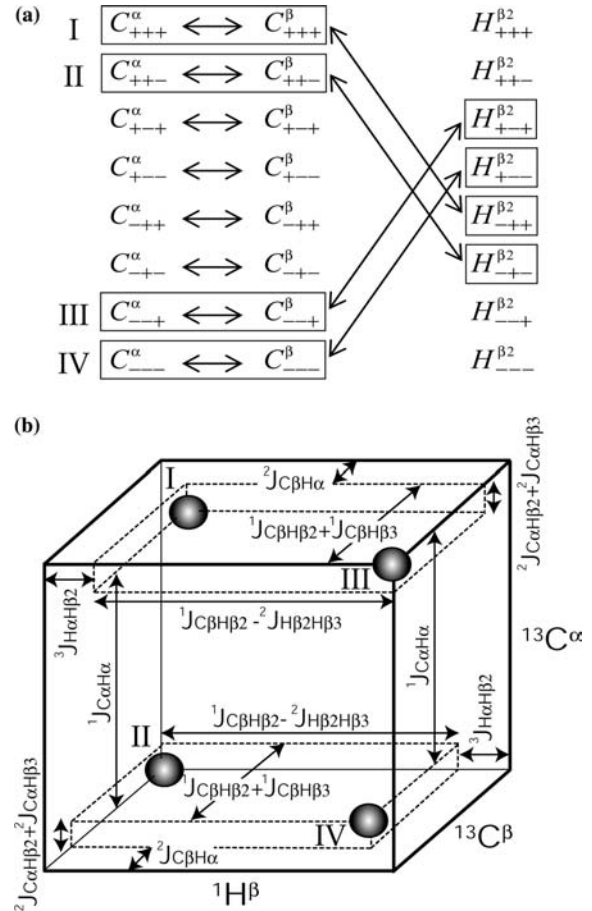


Figure 2. Principle of the 3D spin-state-selective NMR experiment. (a) Diagram showing the correlations between  $^{13}\text{C}^\alpha$ ,  $^{13}\text{C}^\beta$ , and  $^1\text{H}^\beta$  single transitions. Each term  $X_{pqr}$  denotes a transition, where subscripts  $p$ ,  $q$  and  $r$  correspond respectively to the  $^1\text{H}^{\beta 2}$ ,  $^1\text{H}^{\beta 3}$  and  $^1\text{H}^\alpha$  spin states for  $^{13}\text{C}$  transitions ( $X = \text{C}^\alpha$ ,  $\text{C}^\beta$ ), or to  $^{13}\text{C}^\beta$ ,  $^1\text{H}^{\beta 3}$  and  $^1\text{H}^\alpha$  spin states for  $^1\text{H}^{\beta 2}$  transitions ( $X = \text{H}^{\beta 2}$ ). Only the boxed terms are selected, and correspond to the four multiplet components marked I, II, III, IV. (b) Schematic representation of the multiplet pattern obtained in the  $^1\text{H}^\alpha$ -coupled HBCBCA experiment. Multiplet components I, II, III and IV correspond to the combinations of single transitions shown in (a). Double-headed arrows mark the various couplings, appearing as frequency displacements in a given dimension between two components of the multiplet.

defined for  $^1\text{H}^{\beta 2}$ , where  $p$ ,  $q$ , and  $r$  now refer to  $^{13}\text{C}^\beta$ ,  $^1\text{H}^{\beta 3}$  and  $^1\text{H}^\alpha$  eigenstates (and, of course, analogous terms apply for  $^1\text{H}^{\beta 3}$ ). Importantly, the use of a spin state-selective coherence transfer ( $\text{S}^3\text{CT}$ ) between time points  $c$  and  $d$  in Figure 1a transfers  $C_{+-r}^\beta$  into  $H_{+-r}^{\beta 2}$  and  $C_{++r}^\beta$  in  $H_{++r}^{\beta 2}$  (Miclet et al., 2003a, 2004). Finally, as the  $^{13}\text{C}$   $180^\circ$  pulses during the last  $\text{CH}_2\text{-S}^3\text{CT}$  element do not excite  $^{13}\text{C}^\alpha$  nuclei, the overall effect of this last

transfer step acts as a  $360^\circ$  rotation for  $^1\text{H}^\alpha$  spins. This assumption neglects  $T_2$  relaxation and evolution due to couplings other than  $^1J_{C^\alpha H^\alpha}$ , which is a reasonable approximation considering the short durations of  $\tau_1$  and  $\tau_2$ . Thus, connected ( $C_{pqr}^\alpha$ ,  $C_{pqr}^\beta$ ) transitions are then selectively correlated to  $H_{pqr}^\beta$  transitions,  $^1\text{H}^\alpha$  spin states remaining unchanged before and after the CH2-S<sup>3</sup>CT element.

Therefore, the proposed 3D experiment results in four multiplet components for each cross peak, correlating specific  $^{13}\text{C}^\alpha$ ,  $^{13}\text{C}^\beta$  and  $^1\text{H}^\beta$  single transitions as illustrated in Figure 2.

#### *H<sup>4'</sup>-coupled H<sup>5'</sup>C<sup>5'</sup>C<sup>4'</sup> experiment*

For nucleic acids, the  $C^{4'}\text{H}-C^{5'}\text{H}_2$  spin system is very similar to the  $C^\alpha\text{H}-C^\beta\text{H}_2$  spin system in group I amino acids. However, due to the presence of the  $^{13}\text{C}^{3'}$  spin, coupled to  $^{13}\text{C}^{4'}$ , and the crowded nature of the  $C^{5'}\text{H}_2$  region of nucleic acid spectra, some adaptations are used. The pulse scheme (Figure 1b) shows the implementation of a 3D experiment that allows the measurement of eight couplings in nucleic acids:  $^1J_{C^{4'}H^{4'}}$ ,  $^2J_{C^{4'}H^{5'}}$  +  $^2J_{C^{4'}H^{5''}}$ ,  $^2J_{C^{5'}H^{4'}}$ ,  $^1J_{C^{5'}H^{5'}}$ ,  $^1J_{C^{5'}H^{5''}}$ ,  $^2J_{H^{5'}H^{5''}}$ ,  $^3J_{H^{4'}H^{5'}}$ , and  $^3J_{H^{4'}H^{5''}}$ . The experiment is very similar to the one described for proteins, with  $C^{4'}$ ,  $C^{5'}$ ,  $H^{5'}$ , and  $H^{5''}$  being equivalent to  $C^\alpha$ ,  $C^\beta$ ,  $H^{\beta 2}$  and  $H^{\beta 3}$ , respectively. However, taking into account the spectral properties of nucleic acids, the following modifications have been made. First, a S<sup>3</sup>E element (Meissner et al., 1997a,b) has been introduced between point *a* and *b*, selecting only one of the two multiplet components normally observed in the  $^{13}\text{C}^{5'}$  dimension (Miclet et al., 2003b) and therefore requiring that two interleaved experiments be recorded, one for each component. This modification separates the upfield and downfield components of the  $^{13}\text{C}^{5'}-\{\text{H}_2\}$  multiplet into separate subspectra, thereby reducing resonance overlap in the generally poorly dispersed  $^{13}\text{C}^{5'}-^1\text{H}_2$  correlation map. Relaxation losses during the short interval needed for the S<sup>3</sup>E editing are more than compensated by co-adding the  $^{13}\text{C}$  Boltzmann polarization (Brutscher et al., 1998; Pervushin et al., 1998), which under the experimental conditions used (750 MHz; recycle delay of ca. 1 s) can approach 50% of the  $^1\text{H}$  magnetization (Miclet et al., 2004). Also, by setting the pulse phases of the S<sup>3</sup>E selection such that the slowest relaxing, most downfield  $^{13}\text{C}^{5'}$  component is selected, the

INEPT transfer from  $^{13}\text{C}^{5'}$  to  $^{13}\text{C}^{4'}$  (point *b* to *c*) is optimized from a relaxation perspective. Selection of the upfield  $^{13}\text{C}^{5'}-\{\text{H}_2\}$  triplet component is then accomplished by inserting a  $^1\text{H}$   $180^\circ$  pulse (open pulse in Figure 1b), and not by altering the phase of a  $^{13}\text{C}$  pulse in the S<sup>3</sup>E selection. Finally, since no multiple quantum terms are generated in the case of nucleic acids, a constant-time evolution period can be used for the  $^{13}\text{C}^{4'}$  labeling. This makes it possible to decouple  $^1J_{C^{4'}C^{5'}}$  and  $^1J_{C^{4'}C^{3'}}$  without requiring any frequency-selective pulses.

#### *Measurement of couplings*

For convenience, below we only consider the eight couplings that are measured in proteins. However, the discussion is equally applicable to nucleic acids, since  $C^\alpha$ ,  $C^\beta$ ,  $H^{\beta 2}$  and  $H^{\beta 3}$  are equivalent to  $C^{4'}$ ,  $C^{5'}$ ,  $H^{5'}$ , and  $H^{5''}$ , respectively. Each coupling constant is determined by measuring the splitting between two components of the 3D cross peak multiplet (Figure 2). Knowing the description of each cross peak in terms of single transition operators (marked in Figure 2), extraction of coupling constants is straightforward. It is noteworthy that for each methylene group, two multiplets are available, centered at identical frequencies in the  $^{13}\text{C}^\alpha$  and  $^{13}\text{C}^\beta$  dimensions, but with different chemical shift for the two non-equivalent  $^1\text{H}^\beta$ . Therefore, for most of the couplings, two independent measurements are available from the two multiplets. Moreover, as discussed below, each of the couplings can be measured independently from different combinations of multiplet components within a given multiplet, thereby providing additional internal consistency checks.

As follows from Figure 2, the following rules of coupling extraction apply: In the  $^{13}\text{C}^\alpha$  dimension, the difference between peak positions (II–I), gives directly the magnitude of  $^1J_{C^\alpha H^\alpha}$ . Indeed, the corresponding single transition operators,  $C_{+-}^\alpha$  and  $C_{++}^\alpha$ , differ only by their  $^1\text{H}^\alpha$  spin state. Similarly, the difference between peak positions (IV–III) provides a second measurement of this coupling ( $^1\text{H}^{\beta 2}$  and  $^1\text{H}^{\beta 3}$  are in the  $|\beta\rangle$  states for both transitions). The sum  $^2J_{C^\alpha H^{\beta 2}} + ^2J_{C^\alpha H^{\beta 3}}$  is obtained by taking the difference between single transitions ( $C_{--}^\alpha - C_{++}^\alpha$ ) or ( $C_{---}^\alpha - C_{+-}^\alpha$ ), which correspond to cross peaks (III–I) and (IV–II), respectively. Therefore, when taking into account the

presence of the second multiplet, a total of four independent measurements are made for both  ${}^1J_{C\alpha H\alpha}$  and  ${}^2J_{C\alpha H\beta 2} + {}^2J_{C\alpha H\beta 3}$  couplings.

Analogously, in the  ${}^{13}C^\beta$  dimension, the sum  ${}^1J_{C\beta H\beta 2} + {}^1J_{C\beta H\beta 3}$  is obtained from the difference (III–I) and (IV–II), whereas  ${}^2J_{C\beta H\alpha}$  follows from (II–I) to (IV–III). Here again, two measurements per multiplet are made, leading to four independent measurements of each coupling.

In the  ${}^1H$  dimension, depending on the multiplet considered, different couplings are obtained. If centered on the  ${}^1H^{\beta 2}$  chemical shift, cross peaks I and III are characterized by single transitions  $H_{-+}^{\beta 2}$  and  $H_{+-}^{\beta 2}$ , respectively. Therefore, the frequency difference (I–III) corresponds to simultaneous inversions of the spin states of  ${}^{13}C^\beta$  and  ${}^1H^{\beta 3}$ , yielding the difference  ${}^1J_{C\beta H\beta 2} - {}^2J_{H\beta 2 H\beta 3}$ . Similarly, the multiplet centered at the  ${}^1H^{\beta 3}$  chemical shift provides a measurement of  ${}^1J_{C\beta H\beta 3} - {}^2J_{H\beta 2 H\beta 3}$ . Analogously,  ${}^1J_{C\beta H\beta 2} - {}^2J_{H\beta 2 H\beta 3}$  and  ${}^1J_{C\beta H\beta 3} - {}^2J_{H\beta 2 H\beta 3}$  are also obtained by taking the frequency differences in the  ${}^1H^\beta$  dimension of cross peaks (II–IV) within each multiplet. Then, by adding  ${}^1J_{C\beta H\beta 2} - {}^2J_{H\beta 2 H\beta 3}$  and  ${}^1J_{C\beta H\beta 3} - {}^2J_{H\beta 2 H\beta 3}$  and subtracting  ${}^1J_{C\beta H\beta 2} + {}^1J_{C\beta H\beta 3}$ , measured previously in the  ${}^{13}C^\beta$  dimension, the value of  ${}^2J_{H\beta 2 H\beta 3}$  is obtained. Subsequently  ${}^1J_{C\beta H\beta 2}$  and  ${}^1J_{C\beta H\beta 3}$  can be derived. Finally, the frequency displacement II–I (or IV–III) in the  ${}^1H$  dimension corresponds to the inversion of the  ${}^1H^\alpha$  spin state, providing two measurements of  ${}^3J_{H\alpha H\beta 2}$  when observing  ${}^1H^{\beta 2}$ , or  ${}^3J_{H\alpha H\beta 3}$  when observing  ${}^1H^{\beta 3}$ .

As described above, the spin-state selective 3D experiment simultaneously yields values for eight couplings, including heteronuclear  ${}^1J_{CH}$  and  ${}^2J_{CH}$  couplings and homonuclear  ${}^2J_{HH}$  and  ${}^3J_{HH}$  couplings. Previously, alternate methods have been described for measurement of specific subsets of these couplings, usually one single type of coupling per experiment, e.g.  ${}^1J_{CH}$  (Ottiger et al., 1998; Tolman et al., 2001; Ulmer et al., 2003),  ${}^2J_{CH}$  (Duchardt et al., 2001),  ${}^3J_{HH}$  (Grzesiek et al., 1995), but also for simultaneous measurement of  ${}^2J_{HH}$  and  ${}^1J_{CH}$  (Carlomagnano et al., 2000; Miclet et al., 2003). In comparison to these earlier methods, the spin-state selective 3D experiments described here provide many more couplings, albeit for a much smaller selection of spin systems. As will be discussed below, the experiments are largely free of systematic errors and the results are remarkably accurate.

### Precision of the measurements

Before discussing specific sources of artifacts, potentially leading to systematic errors in the measurement of couplings, we first focus on the sensitivity and resolution of the new experiments, which define the attainable precision of the coupling measurements. In the absence of any systematic line shape or phase distortions, the accuracy of a peak position is directly proportional to its signal-to-noise ratio, and inversely proportional to its line width (Kontaxis et al., 2000). Below, we provide a qualitative analysis relative to the “out-and-back” HBCBCA experiment, which uses a sensitivity-enhanced Rance-Kay element, optimized for methylene groups (Schleucher et al., 1994). This latter experiment would allow one to measure one bond  ${}^1J_{C\alpha H\alpha}$  or  ${}^1J_{C\beta H\beta 2} + {}^1J_{C\beta H\beta 3}$  couplings by removing  ${}^1H$  decoupling in the  ${}^{13}C^\alpha$  or  ${}^{13}C^\beta$  dimension, or individual  ${}^1J_{C\beta H\beta 2}$  and  ${}^1J_{C\beta H\beta 3}$  couplings by removing  ${}^{13}C$  decoupling during data acquisition (Olejniczak et al., 1999). Because in our spin-state selective experiments each 3D multiplet consists of four components, the new experiments intrinsically are less sensitive than an experiment where correlation multiplets are simply doublets. To a first approximation, doubling the number of cross peaks halves their intensities, described by a factor  $\lambda_q = 0.5$ . Second, the transfer efficiency of the CH2–S<sup>3</sup>CT is lower compared to a regular Rance-Kay element by a factor  $\lambda_T = 0.85$  (Miclet et al., 2004). However, this loss is more than offset by a gain of up to a factor  $\lambda_J = 2$ , resulting from removal of the geminal  ${}^2J_{H\beta 2 H\beta 3}$  splitting. In cases where the  ${}^2J_{H\beta 2 H\beta 3}$  splitting is unresolved or only partially resolved,  $1 < \lambda_J < 2$ . The CH2–S<sup>3</sup>CT experiment selects correlations with favorable relaxation properties, including the TROSY component of the CH<sub>2</sub> multiplet (cross peaks III and IV in Figure 2) and the most downfield- $H^\beta$ /upfield- $C^\beta$  component (cross peaks I and II in Figure 2), which takes advantage of the large dipole–dipole  $\Gamma_{H^{\beta 2} C^\beta, H^{\beta 2} H^{\beta 3}}^{DD, DD}$  cross-correlated relaxation term. Furthermore, it is possible to estimate the  ${}^1H$  and  ${}^{13}C$  relaxation rates of these four components relative to the corresponding rates in a regular HBCBCA experiment by using experimental rates previously determined for a medium sized system (Miclet et al., 2004), or by calculating such rates for an idealized, isolated spin system (Supporting Information). Selection of

the multiplet components with favorable relaxation properties results in longer  $^1\text{H}$  transverse relaxation times by a factor  $1.3 < \zeta < 1.7$ . Then, assuming that the signal-to-noise-ratio is inversely proportional to the square root of the  $^1\text{H}$  line width and scaled by a factor  $\exp(-R_C T)$ , where  $R_C$  is the  $^{13}\text{C}^\beta$  relaxation rate and  $T$  the constant-time evolution in the  $^{13}\text{C}^\beta$  dimension, the gain in sensitivity relative to a regular  $\text{H}^\alpha$ - or  $\text{H}^\beta$ -coupled HBCBCA experiment can be calculated and typically falls in the  $0.9 < \lambda_\Gamma < 1.5$  range. Thus, the overall ratio of the sensitivity of the spin-state-selective  $\text{H}^\alpha$ -coupled HBCBCA to that of the  $\text{H}^\alpha$ -coupled HBCBCA is given by:

$$\lambda_S = \lambda_J \times \lambda_q \times \lambda_T \times \lambda_\Gamma.$$

For a typical case where  $\tau_c S^2 = 6.7$  ns, and assuming  $\lambda_J = 2$ , one obtains  $\lambda_S^{\text{III,IV}} = 1.34$  (downfield  $^{13}\text{C}^\beta$  components) and  $\lambda_S^{\text{I,II}} = 0.82$  (upfield  $^{13}\text{C}^\beta$  components) when measuring  $^1\text{J}_{\text{C}\alpha\text{H}\alpha}$ , and  $\lambda_S^{\text{III,IV}} = 1.12$ ;  $\lambda_S^{\text{I,II}} = 0.99$  when  $^1\text{J}_{\text{C}\beta\text{H}\beta 2} + ^1\text{J}_{\text{C}\beta\text{H}\beta 3}$  is measured. In practice, somewhat (10–30%) lower numbers are found, mainly resulting from the assumption of a resolved  $^2\text{J}_{\text{H}\beta 2\text{H}\beta 3}$  splitting (implicit in  $\lambda_J = 2$ ) not being quite valid. So, even while all couplings in a given cross peak can be measured from two different combinations of multiplet components, the intrinsic sensitivity and thereby the precision of two such measurements can be very different. For the combination that yields highest sensitivity, the  $\text{CH}_2\text{-S}^3\text{CT}$  HBCBCA experiment typically provides sensitivity comparable to an  $\text{H}^\alpha$ - or  $\text{H}^\beta$ -coupled HBCBCA experiment, while providing far more information.

As described above, in the absence of resonance overlap the spin-state selective  $\text{H}^\alpha$ -coupled HBCBCA experiment provides two measurements for  $^1\text{J}_{\text{C}\beta\text{H}\beta 2} - ^2\text{J}_{\text{H}\beta 2\text{H}\beta 3}$ ,  $^1\text{J}_{\text{C}\beta\text{H}\beta 3} - ^2\text{J}_{\text{H}\beta 2\text{H}\beta 3}$ ,  $^3\text{J}_{\text{H}\alpha\text{H}\beta 2}$  and  $^3\text{J}_{\text{H}\alpha\text{H}\beta 3}$ , and four measurements for  $^1\text{J}_{\text{C}\alpha\text{H}\alpha}$ ,  $^1\text{J}_{\text{C}\beta\text{H}\beta 2} + ^1\text{J}_{\text{C}\beta\text{H}\beta 3}$ ,  $^2\text{J}_{\text{C}\alpha\text{H}\beta 2} + ^2\text{J}_{\text{C}\alpha\text{H}\beta 3}$  and  $^2\text{J}_{\text{C}\beta\text{H}\alpha}$ . Averaging after appropriate weighting to account for the different intensities can further increase the precision of the coupling measurement, as well as provide a warning in case inconsistent results are obtained. The latter situation can result if partial overlap is not recognized during automated spectral analysis.

Small couplings, namely  $^2\text{J}_{\text{C}\alpha\text{H}\beta 2}$  and  $^2\text{J}_{\text{C}\alpha\text{H}\beta 3}$  in the  $^{13}\text{C}^\alpha$  dimension,  $^2\text{J}_{\text{C}\beta\text{H}\alpha}$  in the  $^{13}\text{C}^\beta$  dimension, and  $^3\text{J}_{\text{H}\alpha\text{H}\beta 2}$  and  $^3\text{J}_{\text{H}\alpha\text{H}\beta 3}$  in the  $^1\text{H}$  dimension are generally not resolved in experiments aimed at the

larger  $^1\text{J}_{\text{C}\alpha\text{H}\alpha}$ ,  $^1\text{J}_{\text{C}\beta\text{H}\beta 2}$ ,  $^1\text{J}_{\text{C}\beta\text{H}\beta 3}$  and  $^2\text{J}_{\text{H}\beta 2\text{H}\beta 3}$  couplings. In the absence of spin-state selective coherence transfer, these passive couplings broaden the lines, adversely affecting the precision at which peak positions can be determined. For example, when unresolved, the  $^3\text{J}_{\text{H}\alpha\text{H}\beta}$  coupling causes an apparent line width increase in the  $^1\text{H}$  dimension of up to 12 Hz. Even larger effects are sometimes observed for aligned samples where the  $^1\text{H}^\alpha - ^1\text{H}^\beta$  coupling can be larger. The spin-state selective HBCBCA approach removes these small two- and three-bond splittings, thereby improving the precision of the coupling measurement.

A range of other factors potentially could also influence the values of the measured splittings and thereby adversely influence the accuracy of the measurements. These include imperfections of the selected coherence pathways resulting from pulse miscalibration or mismatching of delays, and relaxation of passive spins. Their effects tend to be quite small, typically much less than 10% of the measured coupling. Cross-correlated relaxation affects the new experiments less than most other methods of coupling measurement. A discussion of these effects is included as supporting information.

#### *Application to GB3*

Eight couplings or combinations thereof have been determined for all but one of the group I residues (C, F, Y, W, D, N, H) in the protein GB3, both under isotropic and weakly aligned conditions. For residue Y33, a complete set of couplings could not be obtained due to the near-degeneracy of the  $\text{H}^{\beta 2}$  and  $\text{H}^{\beta 3}$  resonances. All measurements are included as Supporting Information.

Small regions of selected cross sections through the  $\text{CH}_2\text{-S}^3\text{CT}$  HBCBCA spectra obtained for the protein GB3 under isotropic conditions and in the presence of 10 mg/ml Pf1 phage are presented in Figure 3. The cross sections shown all correspond to residue N37. The values of the dipolar couplings, extracted from the difference in splittings between the spectra recorded under isotropic (Figure 3a) and aligned (Figure 3c) conditions are marked in Figure 3b.

For the 13 group I residues with non-degenerate  $\text{H}^\beta$  resonances in the isotropic GB3 sample, 312 splittings were measured (Supporting Information), corresponding to 104 couplings, with either two or four splittings for each coupling. Note

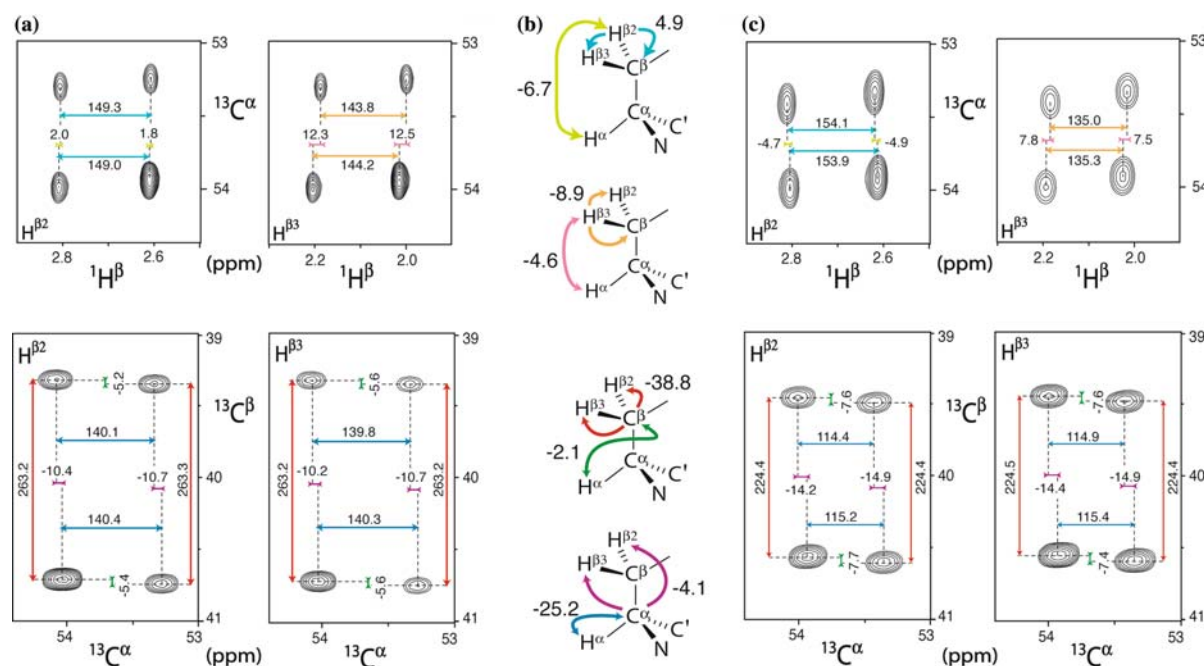


**Figure 3.** Small sections of projected regions of the 3D Spin-State-Selective  $H^2$ -coupled HBCBCA spectra of GB3, recorded in the (a) isotropic and (c) aligned state. The multiplet shown corresponds to N37. The four multiplet components are centered around the chemical shifts of the correlated nuclei (e.g.  $^{13}C^\alpha$ ,  $^{13}C^\beta$ ,  $^1H^\beta$ ). As marked by the double-headed arrows, twelve splittings can be measured per multiplet, which correspond to six different couplings. Twelve additional measurements are made in the second multiplet, leading to a total of 24 splittings for eight couplings. Each color denotes a specific interaction, illustrated in (b). Dipolar couplings derived from the experimental data shown are determined from the difference between the couplings measured in the anisotropic and isotropic phase, and are marked in (b).

that signals from residues other than group I are actively suppressed, in order to minimize spectral congestion. Visual inspection of the spectra indicated that for 23 of the 312 splittings partial overlap could potentially impact the reliability of the measured splittings, and these values were not used in the averaging process. For all other splittings, average values were obtained by weighting each of the two or four available splitting values by the squared inverse of their experimental uncertainty, as derived from the signal-to-noise ratio and line width of the corresponding resonances. Individual values, with their uncertainties and the corresponding averaged values and propagated errors are presented in the Supporting Information. For the majority of couplings, the error falls well below 0.5 Hz.

Several residues yield high values for  $^3J_{H^\alpha H^\beta 2}$  or  $^3J_{H^\alpha H^\beta 3}$  (ca. 12 Hz), with the complementary  $^3J_{H^\alpha H^\beta 3}$  or  $^3J_{H^\alpha H^\beta 2}$  value being small (ca. 2 Hz). The observation that these values are close to the extremes of the range allowed by the corre-

sponding Karplus curves (Haasnoot et al., 1981; Perez et al., 2001) indicates that these residues have their sidechain locked predominately in a single, close to ideally staggered  $\chi_1$  rotamer (Eggenberger et al., 1992). For two residues, N8 and N35, intermediate values in the 6–8 Hz range are observed, indicative of rotameric averaging about the  $\chi_1$  angle.

Our results indicate that the 3D  $CH_2$ - $S^3CT$  HBCBCA experiment provides a useful method for accurate determination of the informative  $^3J_{HH}$  couplings, complementing several alternative methods for measuring these couplings in  $^{13}C$ -enriched proteins (Emerson and Montelione, 1992; Grzesiek et al., 1995). Values of  $^3J_{H^\alpha H^\beta 2}$  and  $^3J_{H^\alpha H^\beta 3}$ , complemented by either  $^3J_{NH^\beta}$ ,  $^3J_{NC^\gamma}$ ,  $^3J_{C^\beta H^\beta}$ ,  $^3J_{C^\gamma C^\gamma}$ , or by  $^1H$ - $^1H$  NOE data can then be used for making stereospecific assignments and determining the sidechain torsion angle  $\chi_1$ . As discussed below, this information can also be obtained directly from the dipolar couplings measured with the 3D  $CH_2$ - $S^3CT$  HBCBCA

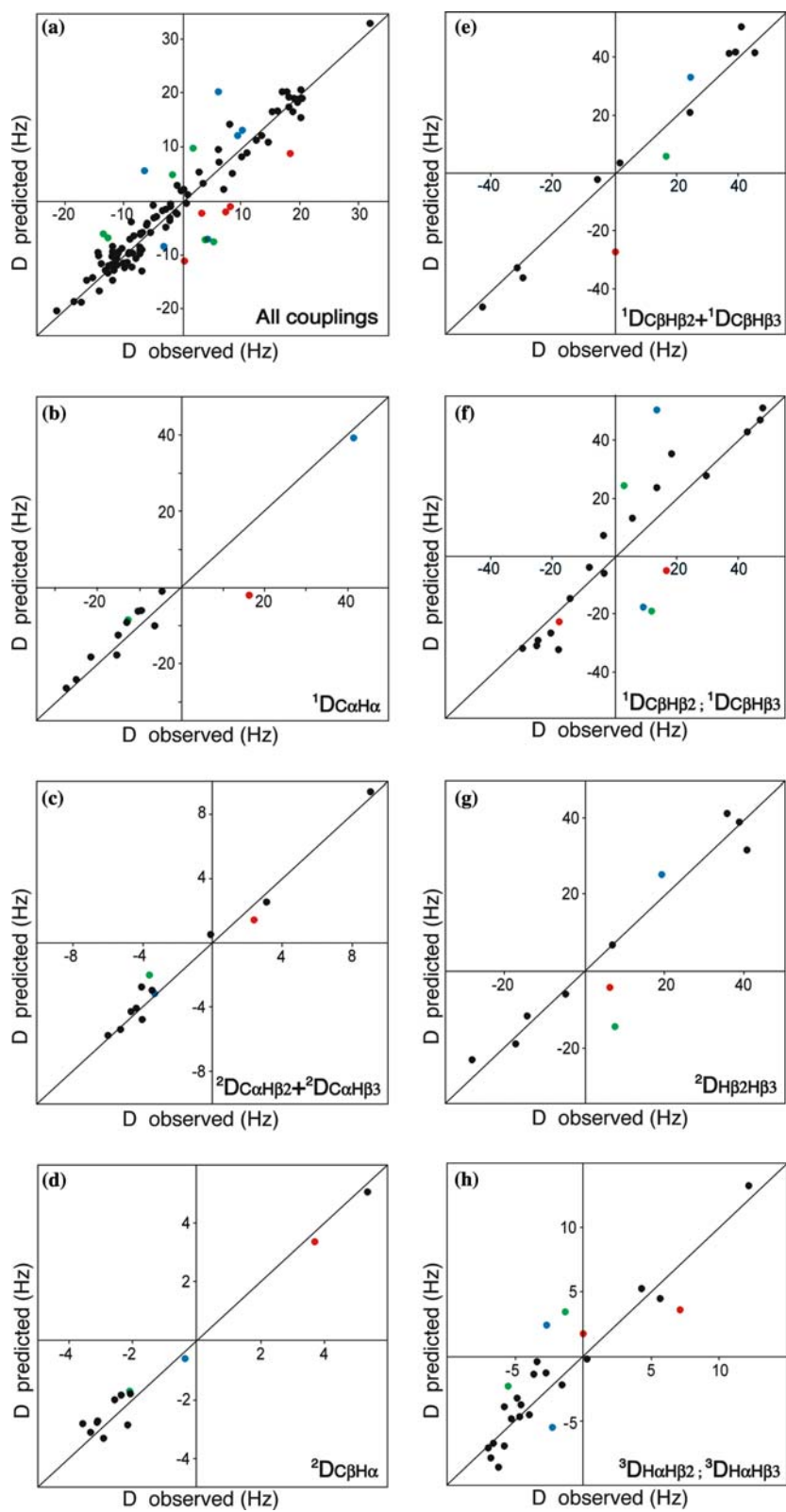


Figure 4. Correlation between observed and predicted residual dipolar couplings,  $D$ , in GB3. Dipolar couplings of mobile residues N8, N35 and D40 are marked in green, blue and red, respectively. Predicted couplings were derived from the NMR-refined X-ray structure (Derrick and Wigley, 1994; Ulmer et al., 2003) (PDB entry 1P7E), using the previously determined alignment tensor orientation in Pf1, but its magnitude scaled by 0.93 to optimize agreement with the  ${}^1D_{C\alpha H\alpha}$  values from the present study. SVD fits of sets containing 8 RDCs, measured for residues Y3, D22, F30, N37, W43, Y45, D46 and D47, to the GB1 structure yields alignment tensors with magnitudes ( $D_a^{CH} = 12.6 \pm 0.7$  Hz) that are in good agreement with the tensor determined from 38  ${}^1D_{C\alpha H\alpha}$  values. (a) Correlation of all eight couplings, normalized to the  ${}^{15}N$ - ${}^1H$  dipolar interaction. (b-h) correspond to  ${}^1D_{C\alpha H\alpha}$ ,  ${}^2D_{C\alpha H\beta 2} + {}^2D_{C\alpha H\beta 3}$ ,  ${}^2D_{C\beta H\alpha}$ ,  ${}^1D_{C\beta H\beta 2} + {}^1D_{C\beta H\beta 3}$ ,  ${}^1D_{C\beta H\beta}$ ,  ${}^2D_{H\beta 2H\beta 3}$  and  ${}^3D_{H\alpha H\beta}$ , respectively. Only couplings  ${}^1D_{C\alpha H\alpha}$  (b) and  ${}^2D_{C\beta H\alpha}$  (d) are independent of the side chain conformation.

experiment, provided that the backbone structure of the protein is known.

Application of the CH2-S<sup>3</sup>CT HBCBCA experiment to the GB3 sample in Pf1 yielded 303 measurable splittings (Supporting Information). Compared to the isotropic sample, the frequency displacement due to the dipolar interaction and the concomitant increase in  ${}^1H$  line width resulted in slightly more resonance overlap for the  ${}^{13}C^\beta$  upfield components of residue F52, making several of its couplings inaccessible. After visual inspection of the spectrum, an additional 16 measurements were excluded because of partial overlap. As a consequence, no reliable values could be determined for the  ${}^1J_{C\beta H\beta 2} - {}^2J_{H\beta 2H\beta 3}$ ,  ${}^1J_{C\beta H\beta 3} - {}^2J_{H\beta 2H\beta 3}$  and  ${}^3J_{H\alpha H\beta 2}$  splittings of residue F52, as well as the  ${}^1J_{C\beta H\beta 3} - {}^2J_{H\beta 2H\beta 3}$  splitting of D36. Therefore, no individual values of  ${}^1J_{C\beta H\beta 2} + {}^1D_{C\beta H\beta 3}$  and  ${}^2J_{H\beta 2H\beta 3} + {}^2D_{H\beta 2H\beta 3}$  were obtained for these two residues. Agreement between the different measurements of a given coupling remains quite good, with propagated errors for the averaged values mostly below 0.5 Hz (Supporting Information). Experimental uncertainties in the  ${}^1J_{C\alpha H\alpha}$  and  ${}^2J_{C\alpha H\beta 2} + {}^2J_{C\alpha H\beta 3}$  displacements are somewhat larger, mainly as a result of the shorter acquisition time used in the  $C^\alpha$  dimension and the lower signal-to-noise ratio.

#### Agreement of RDCs with GB3 X-ray structure

With the exception of two small loop regions, the backbone coordinates of the 1.1-Å resolution X-ray structure of GB3 (Derrick and Wigley, 1994) previously were shown to be in good agreement with the one-bond backbone dipolar couplings, measured in five different alignment media, including Pf1 (Ulmer et al., 2003). The same was found to apply for smaller, multi-bond couplings, measured in a deuterated form of the protein (Meier et al., 2003). The backbone geom-

etry of the X-ray structure was used as a starting point for further refinement on the basis of the dipolar couplings, retaining the sidechain geometries of the X-ray structure, and resulted in only a very small shift (0.32 Å) in backbone coordinates (Ulmer et al., 2003). Here we evaluate agreement between the RDCs involving the sidechain  $H^\beta$  protons and this RDC-refined X-ray structure (PDB entry 1P7E).

Figure 4 compares dipolar couplings measured in the present study with those predicted for the 1P7E structure. For calculating the predicted dipolar couplings, the alignment tensor previously determined for GB3 in Pf1 was used, but its magnitude was scaled to account for the slightly weaker alignment observed in the present sample. On the basis of a comparison of the  ${}^1D_{C\alpha H\alpha}$  values measured in the present study, and those reported by Ulmer et al., (2003), this scaling factor was 0.93. Similarly, 38  ${}^1D_{C\alpha H\alpha}$  values extracted from  ${}^1H$ -coupled 2D CT-HSQC spectra show an excellent linear correlation ( $R_p = 0.998$ , Supporting Information) with the values predicted for the GB3 alignment tensor in Pf1, again with a scaling factor of 0.93. As can be seen in Figure 4 and Table 1, with the exception of three residues (N8, N35 and D40; colored dots in Figure 4) the correlation between the newly measured couplings and values predicted for the GB3 structure is excellent. The side chains of N8 and N35 above already had been shown to be subject to rotameric averaging on the basis of their  ${}^3J_{H\alpha H\beta}$  couplings, and the poor correlation to the refined X-ray structure is therefore not surprising. For D40, the  ${}^3J_{H\alpha H\beta}$  couplings are compatible with a single rotamer ( $\chi_1 = -50 \pm 10^\circ$ ), but this residue is located in a loop region for which both  ${}^{15}N$  relaxation studies and dipolar couplings indicated the presence of significant backbone mobility (Hall and Fushman, 2003; Meier et al., 2003; Ulmer et al., 2003). This residue and its immediate neighbors were therefore

Table 1. Correlation parameters between observed and predicted RDCs in GB3<sup>a</sup>

|            | $^1D_{C\alpha H\alpha}$ | $^2D_{C\alpha H\beta 2} + ^2D_{C\alpha H\beta 3}$ | $^2D_{C\beta H\alpha}$ | $^1D_{C\beta H\beta 2} + ^1D_{C\beta H\beta 3}$ | $^1D_{C\beta H\beta i}$ | $^2D_{H\beta 2 H\beta 3}$ | $^3D_{H\alpha H\beta i}$ |
|------------|-------------------------|---|------------------------|---|-------------------------|---------------------------|--------------------------|
| <i>R</i>   | 0.944                   | 0.986   | 0.989                  | 0.963   | 0.860                   | 0.937                     | 0.905                    |
| <i>R</i> * | 0.972                   | 0.992   | 0.985                  | 0.993   | 0.973                   | 0.987                     | 0.966                    |
| <i>Q</i>   | 0.273                   | 0.254   | 0.145                  | 0.367   | 0.573                   | 0.399                     | 0.369                    |
| <i>Q</i> * | 0.136                   | 0.209   | 0.155                  | 0.174   | 0.281                   | 0.198                     | 0.237                    |
| RMS        | 2.89                    | 2.69  | 1.54                   | 3.88  | 6.06                    | 4.22                      | 3.90                     |
| RMS*       | 1.44                    | 2.21  | 1.64                   | 1.84  | 2.98                    | 2.09                      | 2.50                     |

<sup>a</sup>For each coupling, values of the Pearson's correlation coefficient (*R*), *Q* factors, and RMSD are listed. Parameters marked by an asterisk correspond to those obtained when mobile residues N8, N35 and D40 are excluded from the fit. All RMSD values (in Hz) are normalized to the one-bond  $^1H$ - $^{15}N$  dipolar interaction.

excluded in the previous refinement of the X-ray structure and not only its sidechain, but also its backbone  $^1D_{C\alpha H\alpha}$  couplings agree poorly with this refined structure (Figure 4).

It is noteworthy that for N8 and N35, very good agreement is obtained for couplings  $^1D_{C\alpha H\alpha}$  and  $^2D_{C\beta H\alpha}$ , which do not depend on the  $\chi_1$  angle. Excluding the three residues for which sidechain or backbone mobility is implicated above, the correlations between experimental and predicted dipolar couplings are quite good, albeit slightly lower for the individual  $^3D_{H\alpha H\beta}$  and  $^1D_{C\beta H\beta}$  couplings. As discussed in the *Measurement of couplings* section, these latter couplings are extracted indirectly from the measured splittings and slightly larger errors are therefore not surprising. The correlation for summed  $^2D_{C\alpha H\beta 2} + ^2D_{C\alpha H\beta 3}$  interactions (Figure 4c) is remarkably good, despite the relatively small values of such couplings, but presumably reflects the fact that the sum of these couplings is less sensitive to small changes in  $\chi_1$  angle than most of the other couplings. Therefore, this correlation is less sensitive to small differences in sidechain  $\chi_1$  angle between the solution and crystalline states of the protein. It is likely that minor adjustment of the  $\chi_1$  angle could improve the correlations for the other couplings, but no such refinement has yet been attempted.

#### Application to RNA

For the RNA oligomer, the first nucleotide is not enriched in  $^{13}C$ , but the remaining 23 each show two multiplets for the non-equivalent  $C^{5'}$  protons. Therefore, measurement of up to a maximum of 552 splittings is possible in principle. However, due to the severe spectral crowding in the  $^{13}C^{5'}$  region

and despite the use of a  $S^3E$  element in the pulse sequence, several multiplets are subject to partial overlap (Figure 5). Thus, only 508 splittings could actually be measured for the isotropic sample (Supporting Information). Overlap occurs exclusively in the stem region of the oligomer, but due to the multiple measurements available for a given coupling, a complete set of  $8 \times 23$  couplings was obtained. Uncertainties of individual measurements are greater compared to those obtained for GB3. This is a direct consequence of the approximately three-fold lower signal-to-noise ratio.

Analysis of the  $^3J_{H4'H5'}$  and  $^3J_{H4'H5''}$  data shows uniformly small values, both in the stem and in the loop region, indicative of gauche conformations. Closer inspection of these couplings in the stem region shows that for most residues  $^3J_{H4'H5'} \approx ^3J_{H4'H5''}$ , corresponding to  $\gamma$  angles shifted slightly below the ideally staggered  $\gamma = +60^\circ$  conformation (Blommers et al., 1991; Wijmenga and van Buuren, 1998), in agreement with a statistical analysis of X-ray structures which yields an averaged value of  $\gamma = 55^\circ$  (Murray et al., 2003). Isotropic values for  $^1J_{C5'H5'}$  ( $149.80 \pm 0.83$  Hz) and  $^1J_{C5'H5''}$  ( $147.17 \pm 0.53$  Hz) are highly uniform throughout the oligomer, with  $^1J_{C5'H5'}$  systematically slightly larger than  $^1J_{C5'H5''}$ , as previously noted by Ippel et al. (1996). The oligomer sample in liquid crystalline Pf1 yielded 339 resolved splittings, allowing the determination of all 8 couplings for 70% of the nucleotides. Correlations for stem nucleotides U41, A42, U54-A56, C58, and C59 were insufficiently resolved, primarily as a result of increased line width in the  $^1H$  dimension, caused by homonuclear  $^1H$ - $^1H$  couplings to remote protons. With a Pearson's correlation coefficient of 0.91, the fit of the dipolar couplings for

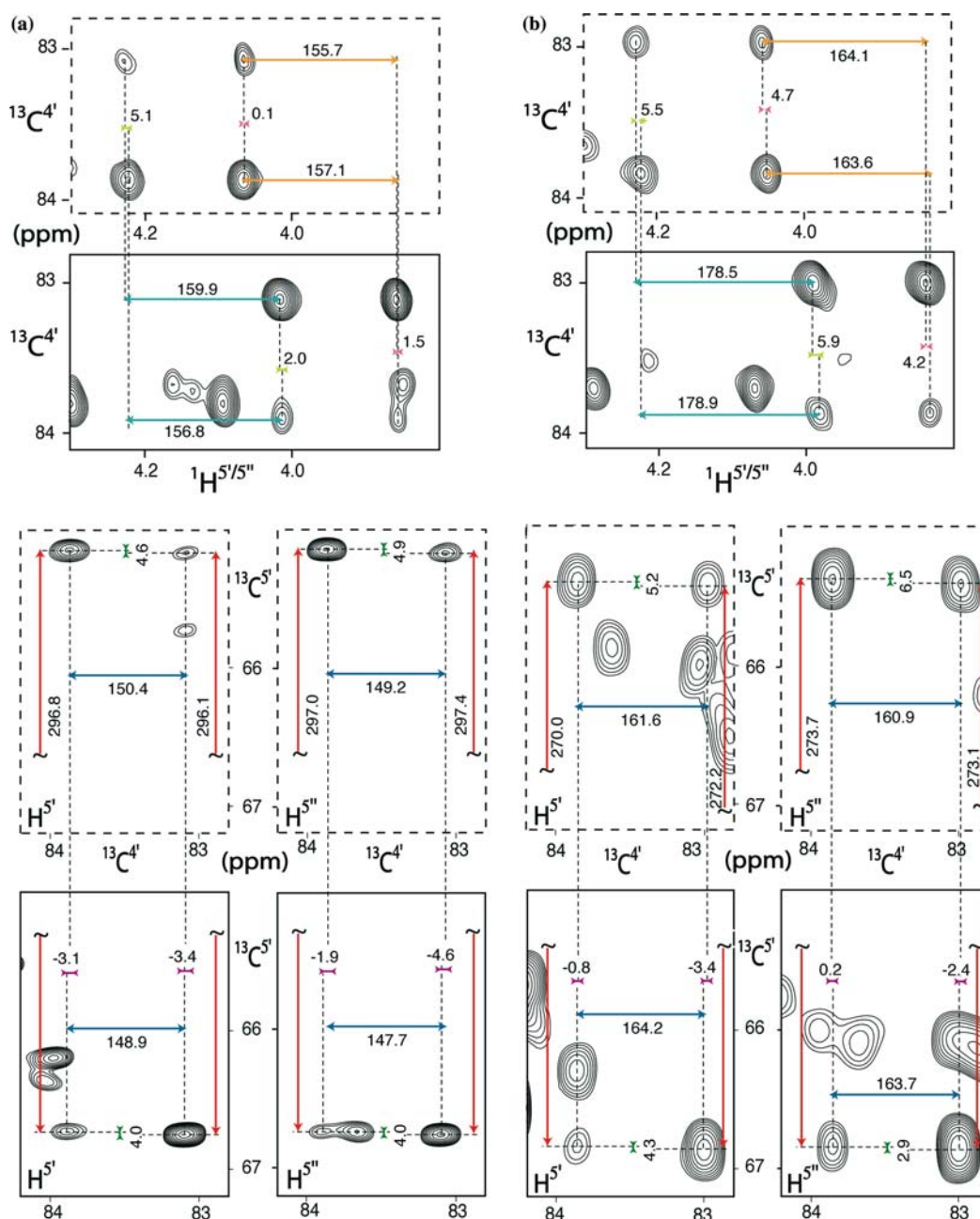


**Figure 5.** Small sections of projected regions of the 750-MHz 3D Spin-State-Selective  $H^4$ -coupled  $H^5C^5C^4$  spectra of the RNA oligomer, recorded in the (a) isotropic and (b) aligned states. The sections shown correspond to the summation of cross-sections through the 3D spectra, selecting correlations for U47. The top two frames for both (a) and (b) correspond to cross sections orthogonal to the  $C^5$  axis, extending from 65.1–65.3 ppm (dashed frame; correlations I and II in Figure 2) to 66.7–66.9 ppm (solid frame; correlations III and IV in Figure 2) through the two separately recorded spectra containing the upfield and downfield components of the  $C^5$  multiplet. The bottom pairs of two frames each correspond to projections of cross sections orthogonal to the  $^1H$  dimension. Projections extend over ca. 0.05 ppm in the  $^1H$  dimension, and are centered at the positions of the  $^1H^{5'}\{-^{13}C^{5'}\}$  and  $^1H^{5''}\{-^{13}C^{5'}\}$  doublet components. Dashed frames correspond to the spectrum containing the upfield  $^{13}C^{5'}$  multiplet component and correlations correspond to peaks I and II in Figure 2; solid frames are for the spectrum with the downfield  $^{13}C^{5'}$  multiplet component and correlations correspond to peaks III and IV in Figure 2. Splittings (marked in Hz) in (a) correspond to  $^1J_{C^5'H^5'} - ^2J_{H^5'H^5''}$  (cyan),  $^3J_{H^5'H^4'}$  (light green),  $^1J_{C^5'H^5''} - ^2J_{H^5'H^5''}$  (orange),  $^3J_{H^5''H^4'}$  (pink),  $^1J_{C^4'H^4'}$  (blue),  $^2J_{C^4'H^5'} + ^2J_{C^4'H^5''}$  (violet),  $^1J_{C^5'H^5''} + ^1J_{C^5'H^5'}$  (red) and  $^2J_{C^5'H^4'}$  (green). The corresponding J + D splittings are marked in panel (b).

the helical stem nucleotides to an idealized A-form helix yields a good correlation (data not shown). As for GB3, comparison of the  $^1D_{C^5'H^5'}$  and  $^1D_{C^5'H^5''}$  couplings predicted for the stem region with measured values identified the downfield proton as  $H^5'$ , consistent with the above noted slight difference in the corresponding  $^1J_{CH}$  values. For the loop, several residues show increased dynamics, and previous measurements indicate that the riboses retain primarily a C3'-endo conformation (O'Neil-Cabello et al., 2004), whereas the  $^3J_{H^4'H^5'}$  couplings are found to be slightly greater than  $^3J_{H^4'H^5''}$ , indicating that  $\gamma$  angles, on average, are slightly lower than in the stem region (ca. 48°) (Blommers et al., 1991; Wijmenga and van Buuren, 1998). With an average of six additional dipolar couplings, available from previous measurements (O'Neil-Cabello et al., 2004), the original and newly measured dipolar couplings can be fit to an idealized C3'-endo ribose with  $\gamma = 50^\circ$ , and either the downfield or the upfield  $C^5'$  proton assigned to  $H^5'$ . For 6 out of the 8 loop nucleotides, this procedure identifies the most downfield resonating proton as  $H^5'$ , which then also agrees with the above noted  $^3J_{H^4'H^5'} < ^3J_{H^4'H^5''}$ . For the two remaining loop nucleotides ( $\psi 46$  and A51), the difference between  $^1D_{C^5'H^5'}$  and  $^1D_{C^5'H^5''}$ , and between  $^3D_{H^4'H^5'}$  and  $^3D_{H^4'H^5''}$  are too small to yield unambiguous stereospecific assignment information for  $H^5'$  and  $H^5''$ . The full set of measured  $J$  and dipolar couplings for the oligomer is presented as Supporting Information.

### Concluding remarks

Spin-state-selective coherence transfer provides an effective method for measurement of scalar and dipolar couplings and allows measurement of eight such couplings for a methine–methylene moiety. Despite the absence of heteronuclear decoupling, which results in four multiplet components for each 3D correlation between three spins, resonance overlap is remarkably low in the application to proteins. In part, this is due to the removal of intra-group  $^1H$ – $^1H$  multiplet splittings, which significantly enhances resolution, but mainly results from the 3D dispersion in the  $^{13}C^\alpha$  and  $^{13}C^\beta$  dimensions. Considering that each splitting is represented either twice ( $^1J_{C^\beta H\beta 2} - ^2J_{H\beta 2 H\beta 3}$ ,  $^1J_{C^\beta H\beta 3} - ^2J_{H\beta 2 H\beta 3}$ ,  $^3J_{H^\alpha H\beta 2}$  and  $^3J_{H^\alpha H\beta 3}$ ) or four

times ( $^1J_{C^\alpha H^\alpha}$ ,  $^2J_{C^\alpha H\beta 2} + ^2J_{C^\alpha H\beta 3}$ ,  $^2J_{C^\beta H^\alpha}$ ,  $^1J_{C^\beta H\beta 2} + ^1J_{C^\beta H\beta 3}$ ) as the displacement of separate pairs of multiplet components, even if partial overlap occurs this usually does not affect all of these pairs. In cases where overlap becomes too extensive, application of the S<sup>3</sup>E filter in Figure 1a (in the same manner as used for nucleic acids in Figure 1b) often will considerably reduce such overlap, at the expense of a longer measuring time. For the 24-nt RNA, used in our study, a complete set of isotropic couplings was extracted, even though the regular 2D CT-HSQC spectrum exhibits extensive overlap.

The ability to measure eight couplings for a methine–methylene moiety opens a range of opportunities, including the evaluation of local mobility (Tolman et al., 2001) and dynamics about the methine–methylene bond, stereospecific assignment of methylene protons, and improving the accuracy of experimental NMR structures. Our results show that even for the very crowded  $C^5'$  region in a 24-nt RNA oligomer, the vast majority of couplings can be measured accurately. In particular, for the eight loop residues in our 24-nt RNA oligomer, where structural restraints are needed most, a complete set of dipolar couplings was obtained. The fact that multiple measurements for each coupling are obtained not only yields an independent method to evaluate their accuracy but also allows averaging of their values to enhance precision. Moreover, if as a result of partial overlap a given splitting is inaccessible, it is likely that its complementary splitting(s) can be measured, adding to the completeness of the acquired data. Although usually measurement of the isotropic reference values is a burdensome prerequisite for extracting dipolar couplings, in the present experiment the isotropic measurement yields two invaluable  $^3J_{HH}$  couplings, which can be readily interpreted in terms of the intervening dihedral angle, complementing the measurement of RDCs.

### Supporting information available

A discussion of potential sources of systematic errors, a table with characteristic relaxation rates, a figure showing the effect of  $^1J_{C^\beta H\beta 2}$  and  $^1J_{C^\beta H\beta 3}$  mismatching on selection of the desired transitions, a figure detailing the dependence of single

transition selection in the  $^1\text{H}$  dimension on J-mismatching, one figure evaluating the error in the  $^3\text{J}_{\text{H}\alpha\text{H}\beta}$  measurement resulting from  $^1\text{H}^\alpha$   $T_2$  relaxation during the transfer of magnetization from  $^{13}\text{C}^\beta$  to  $^1\text{H}^\beta$ , one table containing the splittings measured for GB3 and the RNA oligomer, both in isotropic phase and in Pfl, and the corresponding RDCs. This information is available in electronic form at: <http://dx.doi.org/10.1007/s10858-005-0175-z>.

### Acknowledgements

We thank Erin O'Neil-Cabello for preparing the RNA sample, David Bryce, Alex Grishaev, Chris Jaroniec, Ed Nikonowicz and Tobias Ulmer for extensive discussions, Elena Gustchina for preparing the GB3 sample, and Frank Delaglio for development of special tools facilitating the data analysis.

### References

- Bax, A., Vuister, G.W., Grzesiek, S., Delaglio, F., Wang, A.C., Tschudin, R., and Zhu, G. (1994) *Meth. Enzymol.*, **239**, 79–105.
- Biamonti, C., Rios, C.B., Lyons, B.A., and Montelione, G.T. (1994) *Adv. Biophys. Chem.*, **4**, 51–120.
- Blommers, M.J.J., Vandeven, F.J.M., Vandermaer, G.A., Vanboom, J.H., and Hilbers, C.W. (1991) *Eur. J. Biochem.*, **201**, 33–51.
- Brutscher, B., Boisbouvier, J., Pardi, A., Marion, D., and Sismorre, J.P. (1998) *J. Am. Chem. Soc.*, **120**, 11845–11851.
- Bystrov, V.F. (1976) *Prog. NMR Spectrosc.*, **10**, 41–81.
- Carlomagno, T., Peti, W., and Griesinger, C. (2000) *J. Biomol. NMR*, **17**, 99–109.
- Chou, J.J., Case, D.A., and Bax, A. (2003) *J. Am. Chem. Soc.*, **125**, 8959–8966.
- Clore, G.M., Starich, M.R., and Gronenborn, A.M. (1998) *J. Am. Chem. Soc.*, **120**, 10571–10572.
- Delaglio, F., Grzesiek, S., Vuister, G.W., Zhu, G., Pfeifer, J., and Bax, A. (1995) *J. Biomol. NMR*, **6**, 277–293.
- Derrick, J.P., and Wigley, D.B. (1994) *J. Mol. Biol.*, **243**, 906–918.
- Duchardt, E., Richter, C., Reif, B., Glaser, S.J., Engels, J.W., Griesinger, C., and Schwalbe, H. (2001) *J. Biomol. NMR*, **21**, 117–126.
- Eggenberger, U., Kariminejad, Y., Thuring, H., Ruterjans, H., and Griesinger, C. (1992) *J. Biomol. NMR*, **2**, 583–590.
- Emerson, S.D., and Montelione, G.T. (1992) *J. Am. Chem. Soc.*, **114**, 354–356.
- Emsley, L., and Bodenhausen, G. (1990) *Chem. Phys. Lett.*, **165**, 469–476.
- Geen, H., and Freeman, R. (1991) *J. Magn. Reson.*, **93**, 93–141.
- Griesinger, C., Sørensen, O.W., and Ernst, R.R. (1986) *J. Chem. Phys.*, **85**, 6837–6852.
- Grzesiek, S., Kuboniwa, H., Hinck, A.P., and Bax, A. (1995) *J. Am. Chem. Soc.*, **117**, 5312–5315.
- Haasnoot, C.A.G., Deleeuw, F., Deleeuw, H.P.M., and Altona, C. (1981) *Biopolymers*, **20**, 1211–1245.
- Hall, J.B., and Fushman, D. (2003) *J. Biomol. NMR*, **27**, 261–275.
- Hansen, M.R., Mueller, L., and Pardi, A. (1998) *Nat. Struct. Biol.*, **5**, 1065–1074.
- Hansen, P.E. (1981) *Prog. Nucl. Magn. Reson. Spectrosc.*, **14**, 175–296.
- Ikura, M., Kay, L.E., and Bax, A. (1990) *Biochemistry*, **29**, 4659–4667.
- Ippel, J.H., Wijmenga, S.S., deJong, R., Heus, H.A., Hilbers, C.W., deVroom, E., vanderMarel, G.A., and vanBoom, J.H. (1996) *Magn. Reson. Chem.*, **34**, S156–S176.
- Kay, L.E., Keifer, P., and Saarinen, T. (1992) *J. Am. Chem. Soc.*, **114**, 10663–10665.
- Kontaxis, G., and Bax, A. (2001) *J. Biomol. NMR*, **20**, 77–82.
- Kontaxis, G., Clore, G.M., and Bax, A. (2000) *J. Magn. Reson.*, **143**, 184–196.
- Kuboniwa, H., Grzesiek, S., Delaglio, F., and Bax, A. (1994) *J. Bio. NMR*, **4**, 871–878.
- Marino, J.P., Schwalbe, H., and Griesinger, C. (1999) *Accounts Chem. Res.*, **32**, 614–623.
- Meier, S., Haussinger, D., Jensen, P., Rogowski, M., and Grzesiek, S. (2003) *J. Am. Chem. Soc.*, **125**, 44–45.
- Meiler, J., Blomberg, N., Nilges, M., and Griesinger, C. (2000) *J. Biomol. NMR*, **16**, 245–252.
- Meissner, A., Duss, J.O., and Sorensen, O.W. (1997a) *J. Biomol. NMR*, **10**, 89–94.
- Meissner, A., Duss, J.O., and Sorensen, O.W. (1997b) *J. Magn. Reson.*, **128**, 92–97.
- Miclet, E., O'Neil-Cabello, E., Nikonowicz, E.P., Live, D., and Bax, A. (2003) *J. Am. Chem. Soc.*, **125**, 15740–15741.
- Miclet, E., Williamson, D.C., Clore, G.M., Bryce, D.L., and Bax, A. (2004) *J. Am. Chem. Soc.*, **126**, 10560–10570.
- Mittermaier, A., and Kay, L.E. (2001) *J. Am. Chem. Soc.*, **123**, 6892–6903.
- Montelione, G.T., and Wagner, G. (1989) *J. Am. Chem. Soc.*, **111**, 5474–5475.
- Mueller, G.A., Choy, W.Y., Skrynnikov, N.R., and Kay, L.E. (2000) *J. Biomol. NMR*, **18**, 183–188.
- Murray, L.J.W., Arendall, W.B., Richardson, D.C., and Richardson, J.S. (2003) *Proc. Natl. Acad. Sci. USA*, **100**, 13904–13909.
- O'Neil-Cabello, E., Bryce, D.L., Nikonowicz, E.P., and Bax, A. (2004) *J. Am. Chem. Soc.*, **126**, 66–67.
- Olejniczak, E.T., Meadows, R.P., Wang, H., Cai, M.L., Nettlesheim, D.G., and Fesik, S.W. (1999) *J. Am. Chem. Soc.*, **121**, 9249–9250.
- Ottiger, M., Delaglio, F., Marquardt, J.L., Tjandra, N., and Bax, A. (1998) *J. Magn. Reson.*, **134**, 365–369.
- Perez, C., Lohr, F., Ruterjans, H., and Schmidt, J.M. (2001) *J. Am. Chem. Soc.*, **123**, 7081–7093.
- Permi, P., Rosevear, P.R., and Annala, A. (2000) *J. Biomol. NMR*, **17**, 43–54.
- Pervushin, K.V., Wider, G., and Wuthrich, K. (1998) *J. Biomol. NMR*, **12**, 345–348.
- Prestegard, J.H., Bougault, C.M., and Kishore, A.I. (2004) *Chem. Rev.*, **104**, 3519–3540.
- Ruckert, M., and Otting, G. (2000) *J. Am. Chem. Soc.*, **122**, 7793–7797.

- Sass, H.J., Musco, G., Stahl, S.J., Wingfield, P.T., and Grzesiek, S. (2000) *J. Biomol. NMR*, **18**, 303–309.
- Sass, H.J., Musco, G., Stahl, S.J., Wingfield, P.T., and Grzesiek, S. (2001) *J. Biomol. NMR*, **21**, 275–280.
- Schleucher, J., Schwendinger, M., Sattler, M., Schmidt, P., Schedletzky, O., Glaser, S.J., Sørensen, O.W., and Grisinger, C. (1994) *J. Biomol. NMR*, **4**, 301–306.
- Schmidt, J.M., Blumel, M., Lohr, F., and Ruterjans, H. (1999) *J. Biomol. NMR*, **14**, 1–12.
- Sørensen, O.W., Eich, G.W., Levitt, M.H., Bodenhausen, G., and Ernst, R.R. (1983) *Prog. Nucl. Magn. Reson. Spectrosc.*, **16**, 163–192.
- Tjandra, N., and Bax, A. (1997) *Science*, **278**, 1111–1114.
- Tjandra, N., Grzesiek, S., and Bax, A. (1996) *J. Am. Chem. Soc.*, **118**, 6264–6272.
- Tjandra, N., Omichinski, J.G., Gronenborn, A.M., Clore, G.M., and Bax, A. (1997) *Nat. Struct. Biol.*, **4**, 732–738.
- Tolman, J.R. (2001) *Curr. Opin. Struct. Biol.*, **11**, 532–539.
- Tolman, J.R., Al-Hashimi, H.M., Kay, L.E., and Prestegard, J.H. (2001) *J. Am. Chem. Soc.*, **123**, 1416–1424.
- Tolman, J.R., Flanagan, J.M., Kennedy, M.A., and Prestegard, J.H. (1995) *Proc. Natl. Acad. Sci. USA*, **92**, 9279–9283.
- Tolman, J.R., and Prestegard, J.H. (1996) *J. Magn. Reson. Ser. B*, **112**, 269–274.
- Tycko, R., Blanco, F.J., and Ishii, Y. (2000) *J. Am. Chem. Soc.*, **122**, 9340–9341.
- Ulmer, T.S., Ramirez, B.E., Delaglio, F., and Bax, A. (2003) *J. Am. Chem. Soc.*, **125**, 9179–9191.
- Wang, Y.X., Marquardt, J.L., Wingfield, P., Stahl, S.J., Lee-Huang, S., Torchia, D., and Bax, A. (1998) *J. Am. Chem. Soc.*, **120**, 7385–7386.
- Wijmenga, S.S., and Buuren, B.N.M. van (1998) *Prog. Nucl. Magn. Reson. Spectrosc.*, **32**, 287–387.
- Yang, D.W., Venters, R.A., Mueller, G.A., Choy, W.Y., and Kay, L.E. (1999) *J. Biomol. NMR*, **14**, 333–343.